

RECONCILING DWARF GALAXIES WITH  $\Lambda$ CDM COSMOLOGY:  
SIMULATING A REALISTIC POPULATION OF SATELLITES AROUND A MILKY WAY-MASS GALAXY

ANDREW R. WETZEL<sup>1,2,7,8</sup>, PHILIP F. HOPKINS<sup>1</sup>, JI-HOON KIM<sup>1,3,9</sup>, CLAUDE-ANDRÉ FAUCHER-GIGUÈRE<sup>4</sup>, DUŠAN KERES<sup>5</sup>,  
AND ELIOT QUATAERT<sup>6</sup>

*Draft version December 3, 2024*

ABSTRACT

Low-mass “dwarf” galaxies represent the most significant challenges to the cold dark matter (CDM) model of cosmological structure formation. Because these faint galaxies are (best) observed within the Local Group of the Milky Way (MW) and Andromeda (M31), understanding their formation in such an environment is critical. We present the first results from the Latte Project: the Milky Way on FIRE (Feedback in Realistic Environments). This simulation models the formation of a MW-mass galaxy to  $z = 0$  within  $\Lambda$ CDM cosmology, including dark matter, gas, and stars at unprecedented resolution: baryon mass of  $7070 M_{\odot}$  at spatial resolution down to 1 pc. Latte was simulated using the GIZMO code with a mesh-free method for accurate hydrodynamics and the FIRE model for star formation and explicit feedback within a multi-phase interstellar medium. For the first time, Latte self-consistently resolves the internal structure of dwarf galaxies that form around a MW-mass host down to  $M_{\text{star}} \gtrsim 10^5 M_{\odot}$ . Latte’s population of dwarf galaxies agrees well with those observed in the Local Group across a broad range of properties: (1) distributions of stellar masses and stellar velocity dispersions (dynamical masses), including their joint relation, (2) the mass-metallicity relation, and (3) a diverse range of star-formation histories, including their mass dependence. Thus, Latte produces a realistic population of dwarf galaxies at  $M_{\text{star}} > 10^5 M_{\odot}$  that does *not* suffer from the “missing satellites” or “too big to fail” problems of small-scale structure formation. We conclude that baryonic physics can reconcile observed dwarf galaxies with standard  $\Lambda$ CDM cosmology.

*Subject headings:* cosmology: theory — galaxies: dwarf — galaxies: formation — galaxies: star formation — Local Group — methods: numerical

1. INTRODUCTION

Dwarf galaxies ( $M_{\text{star}} \lesssim 10^9 M_{\odot}$ ) provide the smallest-scale probes of cosmological structure formation and thus are compelling laboratories to test the CDM (cold dark matter) framework. However, observed dwarf galaxies in the Local Group (LG) of the Milky Way (MW) and Andromeda (M31) present significant challenges to CDM. First, the “missing satellites” problem: far fewer luminous satellites appear to be observed around the MW than dark-matter-only models predict (Moore et al. 1999; Klypin et al. 1999). More concretely, the “too big to fail” problem: dark-matter-only simulations predicts too many massive dense subhalos compared with satellites around the MW (Boylan-Kolchin et al. 2011) or M31 (Tollerud et al. 2014). Relatedly, the “core-cusp” problem: the inner density profiles of dwarf galaxies appear to be cored, and not cuspy as CDM predicts (e.g., Simon et al. 2005; Oh et al. 2011). These severe discrepancies are the most important challenges to the CDM model.

Many works thus have explored modifications to standard CDM, such as warm (e.g., Lovell et al. 2014) or self-interacting (e.g., Rocha et al. 2013) dark matter. However, one must account for baryonic physics as well, and many theoretical studies have shown that stellar feedback can drive strong gas inflows/outflows that generate significant cores and reduced dynamical masses in the dark matter of dwarf galaxies (e.g., Read & Gilmore 2005; Pontzen & Governato 2012; Di Cintio et al. 2014; Chan et al. 2015). Almost all such baryonic simulations have been limited to modeling isolated dwarf galaxies, which are computationally tractable at the necessary resolution. However, faint dwarf galaxies are (most robustly) observed only near the MW or M31. Thus, modeling dwarf-galaxy formation within such a host-halo environment is critical, both to understand the role of this environment in their formation and to provide the proper environment to compare statistical properties of the population, such as mass functions, against the LG.

Cosmological simulations of MW-mass galaxies have progressed at increasing resolution and with more realistic stellar physics (e.g., Hopkins et al. 2014; Agertz & Kravtsov 2015; Mollitor et al. 2015), and some simulations have started to resolve the more massive satellite galaxies within MW-mass halos, with promising results (e.g., Brooks & Zolotov 2014; Sawala et al. 2015). However, such simulations have not yet achieved sufficiently high spatial resolution, comparable to simulations of isolated dwarf galaxies, to fully and robustly resolve the *internal* structure of such satellite galaxies, with observed half-light radii as low as  $\sim 200$  pc.

In this Letter, we introduce the Latte Project: the

<sup>1</sup> TAPIR, California Institute of Technology, Pasadena, CA, USA

<sup>2</sup> Carnegie Observatories, Pasadena, CA, USA

<sup>3</sup> Kavli Institute for Particle Astrophysics and Cosmology, Department of Physics, Stanford University, Stanford, CA, USA

<sup>4</sup> Department of Physics and Astronomy and CIERA, Northwestern University, Evanston, IL, USA

<sup>5</sup> Department of Physics, Center for Astrophysics and Space Sciences, University of California at San Diego, La Jolla, USA

<sup>6</sup> Department of Astronomy and Theoretical Astrophysics Center, University of California, Berkeley, CA, USA

<sup>7</sup> Moore Prize Fellow

<sup>8</sup> Carnegie Fellow in Theoretical Astrophysics

<sup>9</sup> Einstein Fellow

Milky Way on FIRE (Feedback in Realistic Environments). The goal of Latte is to simulate a series of MW-mass galaxies to  $z = 0$  within  $\Lambda$ CDM cosmology at parsec-scale resolution, spanning the dynamic range to properly resolve both the host galaxy and the dwarf galaxies that form around it, including state-of-the-art hydrodynamics and FIRE physics to predict their stellar populations. We present first results from our first simulation, focusing on the dwarf-galaxy population.

## 2. LATTE SIMULATIONS

### 2.1. GIZMO code and FIRE model

We run our simulations using the code GIZMO<sup>10</sup> (Hopkins 2015). GIZMO uses a TREE+PM gravity solver updated from GADGET-3 (Springel 2005). For hydrodynamics, we use the mesh-free finite-mass (MFM) method, which is fully Lagrangian and provides automatically adaptive spatial resolution while maintaining machine-level conservation of mass, energy, and momentum, and excellent conservation of angular momentum. MFM simultaneously captures advantages of both Lagrangian smooth-particle hydrodynamics (SPH) and Eulerian adaptive mesh refinement (AMR) schemes. For more details, see Hopkins (2015).

We incorporate radiative cooling and heating rates from CLOUDY (Ferland et al. 2013) across  $10 - 10^{10}$  K, including atomic, molecular, and metal-line cooling for 11 elements. We include ionization/heating from a redshift-dependent, spatially uniform ultraviolet background, including cosmic reionization, from Faucher-Giguère et al. (2009).

We use the FIRE model (Hopkins et al. 2014) for star formation and explicit stellar feedback. Stars form only in locally self-gravitating, molecular gas (Hopkins et al. 2013) with density  $n > 50 \text{ cm}^{-2}$  and with instantaneous efficiency of 100% per free-fall time. FIRE incorporates a comprehensive set of stellar feedback processes: radiation pressure from massive stars, local photoionization and photoelectric heating, core-collapse and Ia supernovae with momentum and thermal energy injection, and stellar winds, all computed from STARBURST99 v7.0 (Leitherer et al. 1999), *with no tuning of parameters*. Previous FIRE cosmological simulations of *isolated* dwarf galaxies have reproduced several key observables: realistic galactic outflows (Muratov et al. 2015),  $M_{\text{star}}$ -metallicity relation (Ma et al. 2016),  $M_{\text{star}}$ -size relation (El-Badry et al. 2015), cored dark-matter profiles (Oñorbe et al. 2015; Chan et al. 2015), inverted age/metallicity gradients (El-Badry et al. 2015), and dispersion-dominated stellar kinematics (Wheeler et al. 2015b).

Starting in this work, we update FIRE’s model for *coupling* feedback to surrounding gas, to ensure that this coupling is isotropic. Previously, FIRE coupled a star particle’s feedback into the nearest  $\approx 32$  gas particles, each receiving a fraction proportional to its kernel volume, regardless of the geometric configuration. We now couple feedback to all gas particles whose kernel encompasses the star particle, with a fraction proportional to the subtended solid angle, and we renormalize each particle’s fraction *along each axis*, so the total initial injection

of mass, energy, and momentum is isotropic around the star particle. We will present full details in Wetzel et al., in prep.

### 2.2. Cosmological Zoom-in Simulations

We cosmologically simulate a MW-mass halo at high resolution using the zoom-in technique (Oñorbe et al. 2014). We first run a dark-matter-only simulation within a periodic volume of length 85.5 Mpc with  $\Lambda$ CDM cosmology:  $\Omega_{\Lambda} = 0.728$ ,  $\Omega_{\text{matter}} = 0.272$ ,  $\Omega_{\text{baryon}} = 0.0455$ ,  $h = 0.702$ ,  $\sigma_8 = 0.807$ , and  $n_s = 0.961$ . We select at  $z = 0$  an isolated halo with  $R_{200\text{m}} = 334 \text{ kpc}$  (within which the mass density is  $200\times$  the average matter density),  $M_{200\text{m}} = 1.3 \times 10^{12} M_{\odot}$  ( $M_{\text{vir}} = 1.1 \times 10^{12} M_{\odot}$ ), and maximum circular velocity  $V_{\text{circ,max}} = 162 \text{ km s}^{-1}$  (these dark-matter halo properties remain the same to within 2% in our full baryonic simulation). This is the same “m12i” halo from Hopkins et al. (2014), and we did not choose it based on its satellite/subhalo population. We trace particles within  $5 R_{200\text{m}}$  back to  $z = 100$  and regenerate the encompassing convex hull at high resolution, embedded within the full lower-resolution volume, using the MUSIC code (Hahn & Abel 2011). Rerun to  $z = 0$ , this zoom-in region has zero low-resolution contamination within  $d_{\text{host}} < 600 \text{ kpc}$  ( $1.8 R_{200\text{m}}$ ).

Our fiducial baryonic simulation contains dark matter, gas, and stars within the zoom-in region, comprising 140 million total particles, with  $m_{\text{dm}} = 3.5 \times 10^4 M_{\odot}$  and  $m_{\text{gas,initial}} = m_{\text{star,initial}} = 7070 M_{\odot}$ . Dark matter and stars have fixed gravitational softening of  $h_{\text{dm}} = 20 \text{ pc}$  and  $h_{\text{star}} = 8 \text{ pc}$  physical. Gas smoothing is fully adaptive and is the same for the hydrodynamic kernel and gravitational softening; the highest resolution achieved is  $h_{\text{gas}} = 1.0 \text{ pc}$ . These softenings allow us to measure properties like velocity dispersions and dynamical masses at our dwarf galaxies’ half-light radii ( $r \gtrsim 200 \text{ pc}$ ) with excellent resolution ( $> 10 h_{\text{dm}}$ ,  $> 25 h_{\text{star}}$ ) (see Klypin et al. 2015; Chan et al. 2015).

We ran this simulation on the Stampede supercomputer using 2048 cores for 22 days (1.1 million CPU hours). To test the effects of baryonic physics and numerical resolution, we also ran (1) a dark-matter-only simulation at the same resolution and (2) a baryonic simulation with  $8\times$  larger particle mass ( $m_{\text{dm}} = 2.8 \times 10^5 M_{\odot}$ ,  $m_{\text{gas,initial}} = 5.7 \times 10^4 M_{\odot}$ ) and  $2\times$  larger force softening.

To identify (sub)halos and their galaxies, we use a modified version of the six-dimensional phase-space halo finder ROCKSTAR<sup>11</sup> (Behroozi et al. 2013), which accounts for multiple species and assigns dark-matter, gas, and star particles to (sub)halos, including the total mass of each within  $R_{200\text{m}}$ .

## 3. RESULTS

We focus on the dwarf galaxies around the MW-mass host at  $z = 0$ , and we will examine the host galaxy in detail in future work. In summary, at  $z = 0$  the host has  $M_{\text{star}} = 9 \times 10^{10} M_{\odot}$  and star-formation rate  $\text{SFR} = 3.5 M_{\odot} \text{ yr}^{-1}$ , compared with  $M_{\text{star}} = 6 \times 10^{10} M_{\odot}$  and  $1.7 M_{\odot} \text{ yr}^{-1}$  for the MW (Licquia & Newman 2015),  $M_{\text{star}} \approx 10^{11} M_{\odot}$  and  $\sim 0.7 M_{\odot} \text{ yr}^{-1}$  for M31 (Tamm et al. 2012; Lewis et al. 2015). The bulge-to-disk mass

<sup>10</sup> <http://www.tapir.caltech.edu/~phopkins/Site/GIZMO>

<sup>11</sup> <https://bitbucket.org/pbehroozi/rockstar-galaxies>

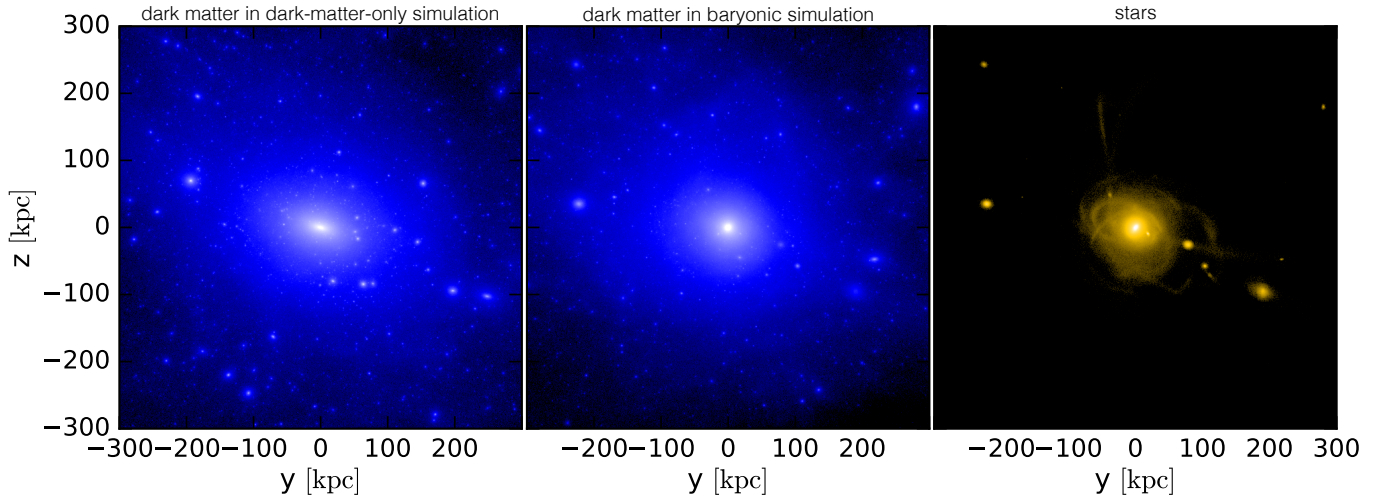


**Figure 1.** Projected mass surface densities of Milky Way-mass host in the Latte simulation at  $z = 0$ : dark matter in the dark-matter-only simulation (left); dark matter (middle) and stars (right) in the baryonic simulation. Color scale is logarithmic, spanning  $10^4 - 10^9 M_{\odot} \text{ kpc}^{-2}$ , same in all panels. Compared with dark-matter-only, the baryonic simulation contains *significantly* ( $\approx 10\times$ ) fewer subhalos at fixed  $V_{\text{circ,max}}$ . Of these subhalos, only 9 host a satellite galaxy with  $M_{\text{star}} > 3 \times 10^5 M_{\odot}$ .

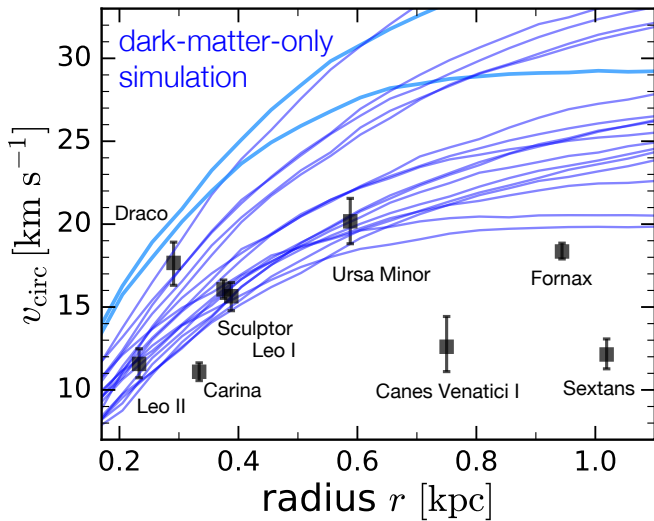


**Figure 2.** Profiles of circular velocity,  $v_{\text{circ}}(r) = \sqrt{Gm_{\text{total}}(<r)/r}$ , for subhalos in the dark-matter-only simulation within  $d_{\text{host}} < 300 \text{ kpc}$  at  $z = 0$ . Points show observed satellites around the MW with  $M_{\text{star}} = 2 \times 10^5 - 2 \times 10^7 M_{\odot}$ , from Wolf et al. (2010). Curves show the 19 subhalos with densities consistent with at least Ursa Minor. Two subhalos (light blue) are denser than all observed satellites; allowing one to host the SMC, one failure remains that is denser than all observed satellites. Of the other subhalos, 5 are consistent with Ursa Minor, Draco, Sculptor, Leo I and II, leading to 13 total failures. Thus, our dark-matter-only simulation suffers from a “too big to fail” problem, consistent with other dark-matter-only simulations.

ratio is 1:2, comparable to M31. Thus, the host’s  $M_{\text{star}}$  is between the MW and M31, with somewhat higher SFR.

At  $z = 0$ , ROCKSTAR identifies 22 dwarf galaxies with  $M_{\text{star}} > 10^5 M_{\odot}$  (our resolution limit) within uncontaminated (sub)halos out to  $d_{\text{host}} = 3 \text{ Mpc}$ . The minimum halo mass for the isolated dwarf galaxies is  $M_{200\text{m}} \approx 10^9 M_{\odot}$ , so our dwarf-galaxy halos are well-resolved with  $\gtrsim 40,000$  dark-matter particles. We define “satellite” and “isolated” galaxies as those at  $d_{\text{host}} < 300 \text{ kpc}$  and  $d_{\text{host}} > 300 \text{ kpc}$ . (We include one galaxy at  $d_{\text{host}} = 367 \text{ kpc}$  as a satellite, because it recently orbited

within  $\approx 0.3 R_{200\text{m}}$ .) The simulation contains 9 satellite and 13 isolated dwarf galaxies.

Figure 1 shows the MW-mass halo at  $z = 0$ , including surface densities down to  $10^4 M_{\odot} \text{ kpc}^{-2}$ . The left panel shows the dark-matter-only simulation, which contains significant substructure. By comparison, dark-matter substructure in the baryonic simulation (middle) is dramatically reduced: within  $d_{\text{host}} < 300 \text{ kpc}$ , it contains  $\approx 10\times$  fewer subhalos at fixed  $V_{\text{circ,max}}$ . Furthermore, Figure 1 (right) shows that, of this reduced population of subhalos, only 9 host a satellite galaxy. Figure 1 (right) also highlights the significant stellar halo, including several streams and shells from disrupting satellites.

To put the importance of baryonic physics in context, we first demonstrate that our dark-matter-only simulation suffers from the “too big to fail” problem (Boylan-Kolchin et al. 2011). We compare with observed dwarf galaxies, compiled in McConnachie (2012), limiting to  $M_{\text{star}} > 10^5 M_{\odot}$ , where observational completeness is well-understood (e.g., Figure 1 in Wetzel et al. 2015). However, we exclude the LMC and M33, because such massive satellites are rare around a MW/M31-mass host (Tollerud et al. 2011; Busha et al. 2011), and we exclude Sagittarius because it is disrupting into a stream.

Figure 2 shows profiles of  $v_{\text{circ}}(r) = \sqrt{Gm_{\text{total}}(<r)/r}$  for satellites within  $d_{\text{host}} < 300 \text{ kpc}$ . Points show observed satellites around the MW with  $M_{\text{star}} = 2 \times 10^5 - 2 \times 10^7 M_{\odot}$ , with well-measured dynamical masses from Wolf et al. (2010). Following Garrison-Kimmel et al. (2014), we show  $v_{\text{circ}}(r)$  curves for the 19 subhalos that are at least as dense as Ursa Minor; these span  $V_{\text{circ,max}} = 20 - 51 \text{ km s}^{-1}$ . Two subhalos (light blue) are denser than all observed satellites. Allowing the highest  $V_{\text{circ,max}}$  subhalo to host the SMC, this leads to one failure that is denser than all observed satellites. Furthermore, counting all other subhalos in Figure 2, and subtracting the 5 that are consistent with Ursa Minor, Draco, Sculptor, Leo I and II, we find 13 total failures that are inconsistent with the MW’s population. These numbers of failures are consistent with the range measured in large samples of MW-mass halos (e.g., Garrison-

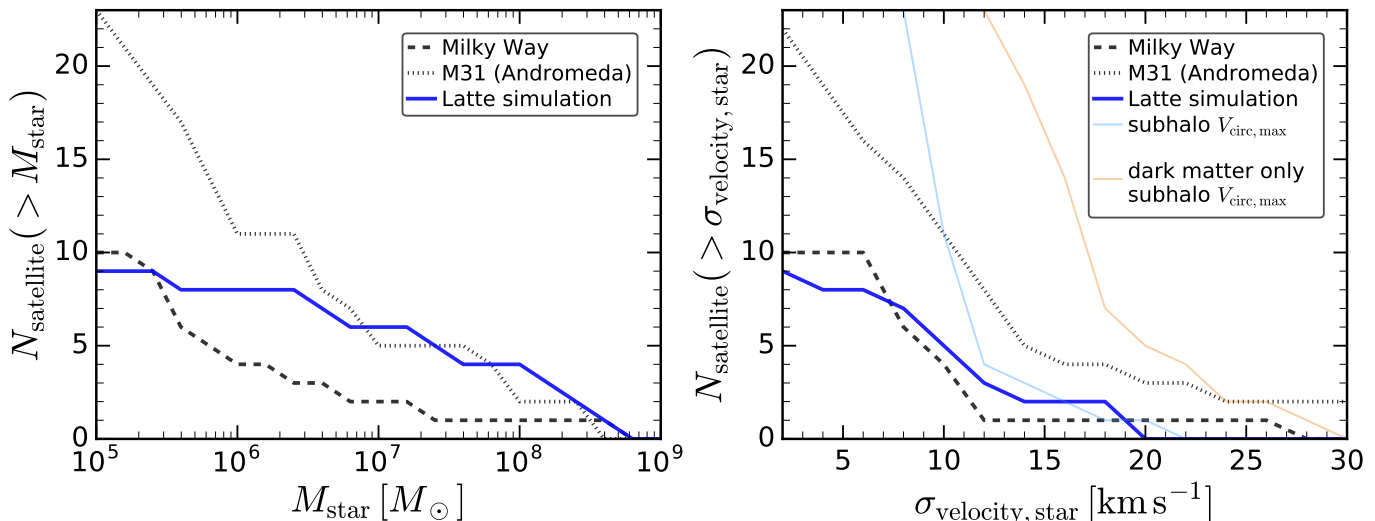


**Figure 3.** Cumulative number of satellite galaxies at  $z = 0$  above a given stellar mass,  $M_{\text{star}}$  (left), and stellar 1D velocity dispersion,  $\sigma_{\text{velocity,star}}$  (right), in the Latte simulation (blue) and observed around the Milky Way (MW; dashed) and Andromeda (M31; dotted) excluding the LMC, M33, and Sagittarius. Thin curves (right) show  $V_{\text{circ,max,1D}} = V_{\text{circ,max}}/\sqrt{3}$  for all dark-matter subhalos in the baryonic (light blue) and dark-matter-only (orange) simulations, demonstrating the  $\approx 10\times$  reduction in subhalo abundance from baryonic physics. Satellite galaxies in the baryonic simulation lie mostly between the MW and M31 at  $M_{\text{star}} \gtrsim 3 \times 10^5 M_{\odot}$  and  $\sigma_{\text{velocity,star}} \gtrsim 7 \text{ km s}^{-1}$ . Above these limits, the Latte simulation is consistent with MW/M31 observations and does not suffer from the “missing satellites” or “too big to fail” problems.

Kimmel et al. 2014; Jiang & van den Bosch 2015). Thus, our dark-matter-only simulation suffers from the “too big to fail” problem.

We next examine dwarf galaxies in the baryonic simulation, demonstrating that they do *not* suffer such problems. Figure 3 (left) shows the cumulative number of satellites above a given  $M_{\text{star}}$ . Blue curves show the baryonic simulation, while black curves show satellites around the MW (dashed) and M31 (dotted). Latte satellite’s  $M_{\text{star}}$  distribution spans  $3 \times 10^5 M_{\odot}$  (similar to Draco) to  $4 \times 10^8 M_{\odot}$  (similar to the SMC) and lies almost entirely between the MW and M31. Overall, Latte’s 9 total satellites agrees well with the 10 satellites  $> 2 \times 10^5 M_{\odot}$  around the MW, so Latte does not suffer from a “missing satellites” problem above this limit.

Figure 3 (right) shows the stellar 1D velocity dispersion,  $\sigma_{\text{velocity,star}}$ , which reflects the total dynamical mass within each galaxy’s stellar radius. Our high spatial resolution allows us to measure this directly and robustly at the half-light radius (Walker et al. 2009), without uncertainties from extrapolating profiles. We compare directly against observed line-of-sight dispersions from Wolf et al. (2010), converting to 1D via  $\sigma_{\text{velocity,star}} = \sigma_{\text{velocity,star,3D}}/\sqrt{3}$ , without having to use  $v_{\text{circ}}(r)$  profiles as in Figure 2 (though we will compare these in future work). Latte’s  $\sigma_{\text{velocity,star}}$  distribution spans  $3.4 - 20 \text{ km s}^{-1}$  and agrees well with the MW at  $\sigma_{\text{velocity,star}} \gtrsim 7 \text{ km s}^{-1}$ . Interestingly, Latte’s high- $M_{\text{star}}$  distribution agrees better with M31, while its high- $\sigma_{\text{velocity,star}}$  distribution agrees better with the MW. However, the joint  $M_{\text{star}} - \sigma_{\text{velocity,star}}$  relation is broadly consistent with observations, as shown below.

For comparison, thin curves in Figure 3 (right) show the distribution of  $V_{\text{circ,max,1D}} = V_{\text{circ,max}}/\sqrt{3}$  for dark-matter subhalos in the baryonic (light blue) and dark-matter-only (orange) simulations. The baryonic simulation contains  $\approx 10\times$  fewer subhalos at fixed  $V_{\text{circ,max}}$ ,

with none above  $V_{\text{circ,max}} = 35 \text{ km s}^{-1}$ . This significant reduction is driven largely by tidal shocking and resonant stripping in the presence of the host’s stellar disk (e.g., D’Onghia et al. 2010; Zolotov et al. 2012, Garrison-Kimmel et al., in prep.). Furthermore, Latte’s satellites have similar  $\sigma_{\text{velocity,star}}$  and  $V_{\text{circ,max,1D}}$ , because FIRE’s feedback produces significant dark-matter cores (Chan et al. 2015).

Next, we further demonstrate that Latte’s dwarf galaxies have realistic internal properties. Figure 4 (top) shows the joint relation between  $\sigma_{\text{velocity,star}}$  and  $M_{\text{star}}$ , for satellite (blue) and isolated (orange) galaxies from the simulation (circles) and observations (stars). Latte’s satellites have somewhat lower  $\sigma_{\text{velocity,star}}$  than its isolated galaxies, with somewhat larger scatter, likely driven by tidal effects (e.g., Zolotov et al. 2012), as we will examine in future work. Most critically, however,  $\sigma_{\text{velocity,star}}$  in both satellite and isolated galaxies agrees well with observations across the  $M_{\text{star}}$  range, primarily because feedback creates dark-matter cores. This result is equally important, because isolated low-mass halos in dark-matter-only simulations also suffer from a “too big to fail” problem compared with the LG (Garrison-Kimmel et al. 2014). Thus, neither satellite nor isolated dwarf galaxies in Latte suffer from a “too big to fail” problem.

The small circles in Figure 4 show the 6 isolated and 2 satellite galaxies in the lower-resolution simulation. Clearly, it resolves isolated galaxies down to  $M_{\text{star}} = 4 \times 10^5 M_{\odot}$ , and indeed, we find that both the  $M_{\text{star}}$  function and the  $M_{\text{star}} - M_{200\text{m}}$  relation are nearly identical for isolated galaxies in the lower- and higher-resolution simulations above this limit. However, the smaller number of satellites in the lower-resolution simulation implies that simulations at this (still high) level of resolution, comparable to the MW-mass halos in Hopkins et al. (2014), struggle to properly resolve satellites within the environment of a MW-mass halo. However, the similarity in the  $\sigma_{\text{velocity,star}} - M_{\text{star}}$  relation at both reso-

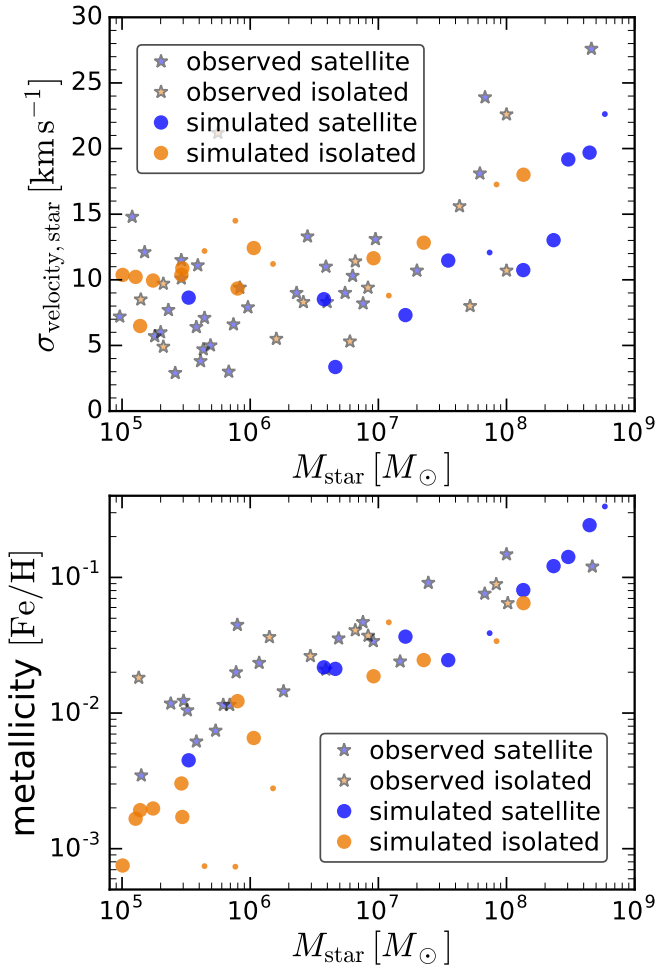


**Figure 4.** Properties of dwarf galaxies versus stellar mass,  $M_{\text{star}}$ , for both satellite ( $d_{\text{host}} < 300$  kpc, blue) and isolated ( $d_{\text{host}} > 300$  kpc, orange) galaxies, in the Latte simulation (circles) and observed around the MW and M31 (stars). Small circles show the lower-resolution simulation. **Top:** Stellar 1D velocity dispersion,  $\sigma_{\text{velocity,star}}$ , scaled to solar,  $[\text{Fe}/\text{H}]$ , compared with observations (Kirby et al. 2013). Latte’s galaxies show a tight relation between  $[\text{Fe}/\text{H}]$  and  $M_{\text{star}}$ , with no offset between satellite and isolated galaxies, as observed.  $[\text{Fe}/\text{H}]$  in Latte agrees with observations, except at  $M_{\text{star}} \lesssim 10^6 M_{\odot}$ , where limited mass-sampling of chemical-enrichment histories becomes significant.

lutions demonstrates that  $\sigma_{\text{velocity,star}}$  is well-resolved in the higher-resolution simulation.

We also examine chemical-enrichment histories via the mass-metallicity relation. Our simulation generates metals via three processes: core-collapse supernovae, Ia supernovae, and stellar winds. Figure 4 (bottom) shows the stellar iron abundance, scaled to solar,  $[\text{Fe}/\text{H}]$ , for both satellite and isolated galaxies. Stars show observed values from Kirby et al. (2013). As is observed, Latte’s galaxies have a tight relation between  $[\text{Fe}/\text{H}]$  and  $M_{\text{star}}$ . Furthermore, satellite and isolated galaxies show *no* offset in  $[\text{Fe}/\text{H}]$ , despite systematic differences in star-formation histories, consistent with observations. While Latte’s galaxies agree well with observations at  $M_{\text{star}} \gtrsim 10^6 M_{\odot}$ , they are lower than observations at

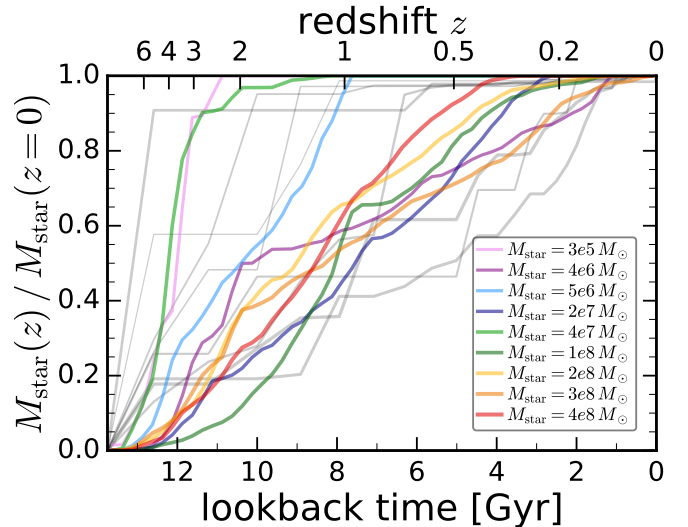


**Figure 5.** Star-formation histories,  $M_{\text{star}}(z)$ , normalized to  $M_{\text{star}}(z=0)$ , for satellite galaxies at  $z=0$ . Colored curves show the Latte simulation, with  $M_{\text{star}}(z=0)$  labeled. Gray curves show observed satellites of the MW (same as Figure 2, excepting Sextans) from Weisz et al. (2014); line thickness indicates  $M_{\text{star}}(z=0)$  across  $2 \times 10^5 - 2 \times 10^7 M_{\odot}$ . Latte’s satellites experienced a broad range of star-formation histories, and all have quenched (turned off) star formation by  $z \approx 0$ , except the second and third most massive. Both trends are consistent with observations in the Local Group.

lower  $M_{\text{star}}$ . However, these galaxies have  $\lesssim 100$  star particles and truncated star-formation histories (see below), so limited mass-sampling of short chemical-enrichment histories likely contributes to reduced  $[\text{Fe}/\text{H}]$ . Indeed, galaxies in the lower-resolution simulation (small circles) have even lower  $[\text{Fe}/\text{H}]$  at  $M_{\text{star}} \lesssim 10^6 M_{\odot}$ , while previous FIRE simulations of isolated dwarf galaxies at even higher resolution show better agreement (Ma et al. 2016).

Finally, Figure 5 shows satellites’ star-formation histories via  $M_{\text{star}}(z)$ , with  $M_{\text{star}}(z=0)$  labeled. Thin gray curves show observed satellites around the MW from Weisz et al. (2014). We compute  $M_{\text{star}}(z)$  based on stellar populations at  $z=0$ , as observations do. Latte’s satellites show a broad range of histories, consistent with observations. Furthermore, satellites with higher  $M_{\text{star}}(z=0)$  formed preferentially later, also consistent with observations. Almost all satellites at  $M_{\text{star}}(z=0) < 10^8 M_{\odot}$  had their star formation quenched (stopped) 3–11 Gyr ago, well after the end of cosmic reionization ( $z \approx 6$ ). However, the second and third most massive satellites remain star-forming to  $z \sim 0$ . This is broadly consistent with the LG, in which only the more massive satellites (SMC, LGS 3, IC 10) remaining star-forming. In future work, we will explore the effects of cosmic reionization, feedback, and the host-halo environment on these star-formation histories.

#### 4. CONCLUSION

We presented first results from the Latte Project: an unprecedentedly high-resolution simulation of a MW-mass galaxy within  $\Lambda$ CDM cosmology, run using GIZMO with the FIRE model for star formation and feedback. Latte produces a realistic population of satellite and isolated dwarf galaxies that are consistent with several observations within the Local Group: (1) distri-

butions of stellar masses and velocity dispersions (dynamical masses), including their joint relation, (2) the  $M_{\text{star}}$ -stellar metallicity relation, and (3) a diverse range of star-formation histories, including their  $M_{\text{star}}$  dependence. Critically, Latte’s dwarf galaxies do *not* suffer the “missing satellites” or “too big to fail” problems of small-scale structure formation, down to  $M_{\text{star}} \gtrsim 10^5 M_{\odot}$  and  $\sigma_{\text{velocity,star}} \gtrsim 7 \text{ km s}^{-1}$ . Because our dark-matter-only simulation does suffer from both, we conclude that baryonic physics can account for the observed population in the Local Group and thus can reconcile dwarf galaxies with standard  $\Lambda$ CDM cosmology.

This agreement with observations arises for primarily two reasons. First, as Oñorbe et al. (2015) and Chan et al. (2015) demonstrated for isolated dwarf galaxies, FIRE’s stellar feedback can generate significant dark-matter cores, reducing their dynamical masses and thus stellar velocity dispersions. Second, our baryonic simulation contains *significantly* ( $10\times$ ) fewer subhalos at fixed  $V_{\text{circ,max}}$  within  $d_{\text{host}} < 300 \text{ kpc}$ , because the host’s stellar disk acts to destroy (already cored) subhalos, as we will quantify in Garrison-Kimmel et al., in prep. (also, Zolotov et al. 2012). Additionally, many lower-mass subhalos contain no stars or gas and are completely dark. However, our current simulation cannot resolve galaxies with  $M_{\text{star}} < 10^5 M_{\odot}$ . As we push Latte to even higher resolution, we expect that lower-mass subhalos will host faint and ultra-faint galaxies (e.g., Wheeler et al. 2015a), providing theoretical insight for the burgeoning population being discovered around the MW (e.g., Koposov et al. 2015; Drlica-Wagner et al. 2015).

We thank Andrew Benson, Mike Boylan-Kolchin, James Bullock, Alis Deason, Shea Garrison-Kimmel, Marla Geha, Evan Kirby, Robyn Sanderson, Josh Simon, Erik Tollerud, Risa Wechsler for enlightening discussions, Dan Weisz for sharing observations, and Peter Behroozi for sharing ROCKSTAR. A.R.W. acknowledges support from the Moore Center for Theoretical Cosmology and Physics at Caltech. P.F.H. was supported by a Sloan Research Fellowship, NASA ATP Grant NNX14AH35G, and NSF Collaborative Research grant #1411920 and CAREER grant #1455342. J.K. acknowledges support from NASA through an Einstein Postdoctoral Fellowship, grant PF4-150147. C.A.F.G. was supported by NSF grants AST-1412836 and AST-1517491, NASA grant NNX15AB22G, and STScI grant HST-AR-14293.001-A. D.K. was supported by NSF grant AST-1412153 and funds from UCSD. E.Q. was supported by NASA ATP grant 12-APT12-0183 and a Simons Investigator award from the Simons Foundation. Our simulations used computational resources via the Extreme Science and Engineering Discovery Environment (XSEDE), supported by NSF.

## REFERENCES

- Agertz, O., & Kravtsov, A. V. 2015, ArXiv e-prints, arXiv:1509.00853  
 Behroozi, P. S., Wechsler, R. H., & Wu, H.-Y. 2013, ApJ, 762, 109  
 Boylan-Kolchin, M., Bullock, J. S., & Kaplinghat, M. 2011, MNRAS, 415, L40  
 Brooks, A. M., & Zolotov, A. 2014, ApJ, 786, 87  
 Busha, M. T., Wechsler, R. H., Behroozi, P. S., et al. 2011, ApJ, 743, 117  
 Chan, T. K., Kereš, D., Oñorbe, J., et al. 2015, MNRAS, 454, 2981  
 Di Cintio, A., Brook, C. B., Macciò, A. V., et al. 2014, MNRAS, 437, 415  
 D’Onghia, E., Springel, V., Hernquist, L., & Keres, D. 2010, ApJ, 709, 1138  
 Drlica-Wagner, A., Bechtol, K., Rykoff, E. S., et al. 2015, ApJ, 813, 109  
 El-Badry, K., Wetzel, A. R., Geha, M., et al. 2015, ArXiv e-prints, arXiv:1512.01235  
 Faucher-Giguère, C.-A., Lidz, A., Zaldarriaga, M., & Hernquist, L. 2009, ApJ, 703, 1416  
 Ferland, G. J., Porter, R. L., van Hoof, P. A. M., et al. 2013, RMxAA, 49, 137  
 Garrison-Kimmel, S., Boylan-Kolchin, M., Bullock, J. S., & Kirby, E. N. 2014, MNRAS, 444, 222  
 Hahn, O., & Abel, T. 2011, MNRAS, 415, 2101  
 Hopkins, P. F. 2015, MNRAS, 450, 53  
 Hopkins, P. F., Kereš, D., Oñorbe, J., et al. 2014, MNRAS, 445, 581  
 Hopkins, P. F., Narayanan, D., & Murray, N. 2013, MNRAS, 432, 2647  
 Jiang, F., & van den Bosch, F. C. 2015, MNRAS, 453, 3575  
 Kirby, E. N., Cohen, J. G., Guhathakurta, P., et al. 2013, ApJ, 779, 102  
 Klypin, A., Kravtsov, A. V., Valenzuela, O., & Prada, F. 1999, ApJ, 522, 82  
 Klypin, A., Prada, F., Yepes, G., Heß, S., & Gottlöber, S. 2015, MNRAS, 447, 3693  
 Koposov, S. E., Belokurov, V., Torrealba, G., & Evans, N. W. 2015, ApJ, 805, 130  
 Leitherer, C., Schaerer, D., Goldader, J. D., et al. 1999, ApJS, 123, 3  
 Lewis, A. R., Dolphin, A. E., Dalcanton, J. J., et al. 2015, ApJ, 805, 183  
 Licquia, T. C., & Newman, J. A. 2015, ApJ, 806, 96  
 Lovell, M. R., Frenk, C. S., Eke, V. R., et al. 2014, MNRAS, 439, 300  
 Ma, X., Hopkins, P. F., Faucher-Giguère, C.-A., et al. 2016, MNRAS, 456, 2140  
 McConnachie, A. W. 2012, AJ, 144, 4  
 Mollitor, P., Nezri, E., & Teyssier, R. 2015, MNRAS, 447, 1353  
 Moore, B., Ghigna, S., Governato, F., et al. 1999, ApJ, 524, L19  
 Muratov, A. L., Kereš, D., Faucher-Giguère, C.-A., et al. 2015, MNRAS, 454, 2691  
 Oñorbe, J., Boylan-Kolchin, M., Bullock, J. S., et al. 2015, MNRAS, 454, 2092  
 Oñorbe, J., Garrison-Kimmel, S., Maller, A. H., et al. 2014, MNRAS, 437, 1894  
 Oh, S.-H., Brook, C., Governato, F., et al. 2011, AJ, 142, 24  
 Pontzen, A., & Governato, F. 2012, MNRAS, 421, 3464  
 Read, J. I., & Gilmore, G. 2005, MNRAS, 356, 107  
 Rocha, M., Peter, A. H. G., Bullock, J. S., et al. 2013, MNRAS, 430, 81  
 Sawala, T., Frenk, C. S., Fattahi, A., et al. 2015, ArXiv e-prints, arXiv:1511.01098  
 Simon, J. D., Bolatto, A. D., Leroy, A., Blitz, L., & Gates, E. L. 2005, ApJ, 621, 757  
 Springel, V. 2005, MNRAS, 364, 1105  
 Tamm, A., Tempel, E., Tenjes, P., Tihhonova, O., & Tuvikene, T. 2012, A&A, 546, A4  
 Tollerud, E. J., Boylan-Kolchin, M., Barton, E. J., Bullock, J. S., & Trinh, C. Q. 2011, ApJ, 738, 102  
 Tollerud, E. J., Boylan-Kolchin, M., & Bullock, J. S. 2014, MNRAS, 440, 3511  
 Walker, M. G., Mateo, M., Olszewski, E. W., et al. 2009, ApJ, 704, 1274  
 Weisz, D. R., Dolphin, A. E., Skillman, E. D., et al. 2014, ApJ, 789, 147  
 Wetzel, A. R., Tollerud, E. J., & Weisz, D. R. 2015, ApJ, 808, L27  
 Wheeler, C., Oñorbe, J., Bullock, J. S., et al. 2015a, MNRAS, 453, 1305  
 Wheeler, C., Pace, A. B., Bullock, J. S., et al. 2015b, ArXiv e-prints, arXiv:1511.01095  
 Wolf, J., Martinez, G. D., Bullock, J. S., et al. 2010, MNRAS, 406, 1220  
 Zolotov, A., Brooks, A. M., Willman, B., et al. 2012, ApJ, 761, 71